A New Compact Optical System Proposal and Image Quality Comparison Against Other Affordable Non-mydriatic Fundus Cameras

David Melo[1,2(✉)], Filipe Soares[2], Simão Felgueiras[2], João Gonçalves[2], and Pedro Vieira[1]

[1] Department of Physics, Faculdade de Ciências e Tecnologia, Universidade Nova de Lisboa, Quinta da Torre, 2829-516 Caparica, Portugal
ds.melo@campus.fct.unl.pt
[2] Fraunhofer Portugal AICOS, Rua Alfredo Allen, 455/461, 4200-135 Porto, Portugal

Abstract. Imaging the eye retina is critical to diagnose various pathologies, particularly Diabetic Retinopathy, which is the leading cause of avoidable blindness in the world. The image acquisition through table-top fundus cameras is the preferred method for retinopathy screening. However, these devices require expertise for operation, limiting its broad application. In this paper, two handheld fundus camera prototypes developed by Fraunhofer AICOS (EyeFundusScope Compact and EyeFundusScope Standard) have their optical capabilities compared, not only between each other but also with another commercially available camera. Field-of-view measurements are performed, as well as a subjective analysis on eye model images acquired with each of prototypes. Besides the comparison between handheld devices in the same experimental setup, conceptual specification on the prototype and optical system for the Compact version are described in order to demonstrate the most relevant issues to be considered when developing a valuable instrument for diabetic retinopathy screening and diagnosis.

Keywords: Diabetic retinopathy · Fundus camera design · Handheld devices

1 Introduction

1.1 Diabetic Retinopathy

The eye retina is the only structure in the body where vessels can be directly seen, without intrusive procedures. Imaging this structure is extremely important in the diagnosis of various pathologies, particularly Diabetic Retinopathy. This is a microvascular disease caused by the diabetes mellitus condition, affecting 76% of the diabetic patients for longer than 20 years [6] and being the leading cause of blindness in adults with working age [5]. It is characterized by the loss of perycites

A. Cliquet jr. et al. (Eds.): BIOSTEC 2018, CCIS 1024, pp. 26–48, 2019.
https://doi.org/10.1007/978-3-030-29196-9_2

and by a progressive capillary occlusion that occurs mostly without symptoms. The capillary occlusion can lead to retinal ischemia and to the breakdown of the blood-retinal-barrier [28].

The disease can be divided in two different stages: Non-proliferative and Proliferative [15]. The first is characterized by abnormalities in the blood vessels materialized in the leakage of substances from the lumen of the vessels to the retinal epithelium. The leakages may be the blood itself leading to microaneurysms and intraretinal hemorrhages, and lipids leading to hard and soft Exudates [8,10,15]. The Proliferative stage is characterized by the creation of new blood vessels surrounding occluded regions (neovascularization). The new blood vessels, being more fragile than the previous ones, increase the risk of bleeding and do not solve retinal ischemia [10]. In the Proliferative stage there is also the formation of fibrous tissue that while contracting can provoke retinal detachment [23].

Several types of instruments can perform ophthalmological examination, but for the diagnosis of Diabetic Retinopathy the use of Fundus Camera is preferred [25].

The asymptomatic profile of the initial progression of diabetic retinopathy is problematic for diagnostic purposes. On the other hand, the success of early treatment provides a large incentive to implement population-based screening programs for diabetic patients. In these programs, images of the patient retinas are acquired and assessed by qualified technicians and ophthalmologists, which lead to high costs due to the required use of expensive and bulky equipment, and the laborious task of manual analysis by scarcely available medical personnel. The prototypes EyeFundusScope, currently under investigation by Fraunhofer Portugal AICOS, aims to address these issues by researching on a self-contained solution comprising automated retinopathy detection with a low cost optical attachment to a smartphone for retinal image acquisition. The major goal is to improve patient access to early treatment and decrease the burden of screening actions on healthcare systems, mainly in medically underserved areas. The prototype described in this paper being compact, easy to transport, easy to mount and revealing good image quality can be a good tool for the accomplishment of these objectives.

1.2 Fundus Camera

A Fundus Camera is a device that allows the observation of the structures and the blood vessels in the ocular fundus, being employed in the diagnosis of several pathologies (like Diabetic Retinopathy, described in Sect. 1.1) [21].

When compared with other eye examination devices, a Fundus Camera enables patient documentation and easy follow, as well as allowing analysis of a great extent of the patient retina, due to the wide field-of-view empowered by the usage of indirect ophthalmoscopy principles, hardly achievable with direct ophthalmoscopy methods [2,22].

The importance of the fundus examination can be seen in many medicine fields and not only in ophthalmology. Since the retina is the human body struc-

ture where the vessels can more easily be seen with no use of ionizing radiation [21], fields like Neurology and Cardiology can also use the capabilities of a Fundus Camera [19]. A handheld portable Fundus Camera can also be a crucial tool in the development of telemedicine [21].

In this work, to diminish the production costs, only the fundamental components of a Fundus Camera were used. When compared with the version presented in Melo et al. on the paper "Optical Design of a Compact Image Acquisition Device for Mobile Diabetic Retinopathy Screening", [17] the final optical system used in the compact version of the prototype has some improvements. To prevent the existence of brighter spots in the final image obtained, circular polarizers were added to the optical path avoiding that light reflected from the cornea or from the back of the objective lens could reach Smartphone CMOS and an iris (or aperture stop) to limit the smartphone angle of view only to the required for a 40°. The usefulness of polarizers in ophthalmology, specifically in fundus imaging will be discussed in the Sect. 2.4. The software used for the Optical Simulation was BEAM IV, an Optical Ray Tracer developed by Stellar Software. Figure 1 shows a diagram with the refractive components that are fundamentally present in a Fundus Camera.

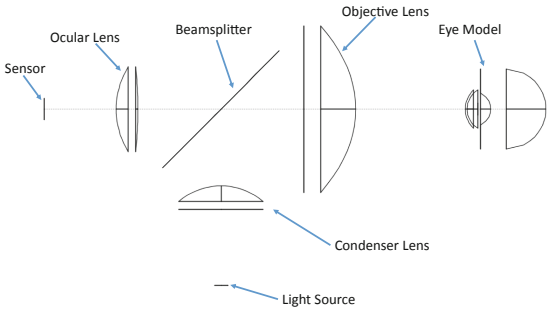

Fig. 1. Demonstration of the fundamental components in the Fundus Camera prototype [17].

The usage of smartphone cameras as sensors is justified by its continuous evolution. An evolution on the sensor can lead to a better image quality, and consequently to an improved performance on the image analysis algorithms, associated with the smartphone applications.

1.3 Optical Principles

To reach an optimal optical system several lenses types were tested. To simulate them according to the characteristics supplied by the manufacturers, the thin lens approximation was used. This approximation neglects the thickness of the lens and considers that the unit planes pass through the axial point of the infinitely thin lens [13]. Considering that the media on both sides of the lens is the same, the following equation can be used to describe it [3].

Lens-Maker's Formula

$$P_{lens} = \frac{n_{lens} - n_0}{n_0}\left(\frac{1}{R_1} - \frac{1}{R_2}\right) \quad (1)$$

Where n_0 is the refractive index of the surrounding medium, the air in this case, equal to 1, n_{lens} is the refractive index of the lens, R_1 is the radius of curvature of the first surface and R_2 is the radius of curvature of the second surface. The P_{lens} is the refractive power in diopters.

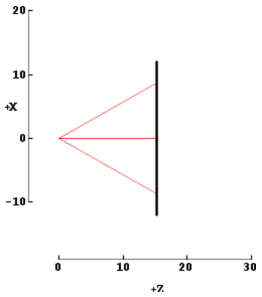

Fig. 2. Demonstration of the 4-extremes model along the x-axis [17].

To simulate a Fundus Camera optical system, the optical path taken by the rays is separated in two different ones by the usage of a beamsplitter [30]. The path that describes how the rays illuminate the retina is called *illumination path* and the path describing how the rays go from the retina to the smartphone camera is called *imaging path*. To simulate them two different approaches were tested, the *4-extreme model* for the illumination, and the *parallel rays model* for the imaging path (see Fig. 2). The 4-extreme model assumes that the light source emits from a single point with a certain aperture previously declared by the manufacturer. The angles for which the relative luminous intensity is bellow half the maximum intensity can be neglected.

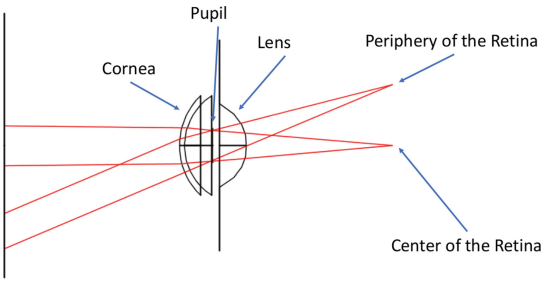

Fig. 3. Demonstration of the parallel rays model. In this figure rays are focused on the retina, leaving the pupil collimated and parallel [17].

The parallel rays model assumes that when two rays focused at some point reach a lens they are collimated and leave the lens with the same direction and parallel with each other. In Fig. 3 one of the applications of this model is demonstrated, showing rays focused at some point, leaving the pupil parallel.

1.4 Related Work

Recently, the features of handheld Fundus Camera prototypes have increased significantly when compared with the traditional tabletop fundus cameras [30], proving as an helpful instrument in the diagnosis of many pathologies related with the retina and facilitating telemedicine applications [14,24]. This improvement of the capabilities of handheld devices led to a variety of different approaches. Some examples that reflect the recent scientific development are:

- Nonmydriatic Fundus Camera Based on the Raspberry Pi® Computer: Uses the Raspberry Pi® camera module coupled with a Condenser Lens to perform fundus imaging with a very low production cost [26].
- Eye-Selfie: By using internal fixation points as targets, it allows a self-performed acquisition of the fundus photography, completely by the patient [27].

There are already, some fundus imaging devices available in the market but most, present one of the following issues:

- Low Field Of View, as for the D-EYE ophthalmoscope [9].
- Require pupil dilation, as for the Volk inView [32].
- High price, as for the Volk Pictor Plus [33].

This year, Optomed commercialized a new device for fundus imaging named Optomed Aurora [18]. It presents better features than any other fundus camera available, showing a Field-of-View of $50 \times 40°$. To ensure that the examiner capability for identification of eye smallest structures isn't diminished by increasing the Field-of-view, a screen correspondingly large is used. Besides fundus imaging, the fundus camera also allows the observation of the surface of the eye and surrounding areas. This way it is versatile enough to be an exceptional tool for the screening of eye diseases. The User Interface comprises a rotary encoder, capacitive touch buttons and battery charging indicator LEDs.

The selection of the OICO Fundus Camera for the comparison tests described in the Sect. 3 is justified by its similarities with EFS prototypes, namely its low-cost, high availability and by the usage of the smartphone camera for acquisition of the fundus images.

OICO fundus camera presents as main features:

- Field-of-View: 35°
- Sensor Resolution: 12 Megapixel
- Minimum Pupil Size: 3.4 mm
- Capture Mode: Infrared for guidance and Color for acquisition

The system we propose differs from the previous approaches by using a smartphone for non-mydriatic, high field-of-view retinal image acquisition. The use of a smartphone instead of custom electronic devices for image capture and processing allows a substantial decrease in costs while allowing for a very high image quality and resolution, thus guaranteeing the cost-effectiveness of the overall solution.

2 Compact System Design

2.1 Eye Model

To guarantee a satisfactory field-of-view, an accurate model of the eye is needed. The eye has two refractive lenses, the cornea and the crystalline lens. Based on literature [1] and following a similar approach to [29], a model of the eye was created in BEAM IV considering the radius of curvature, diameter and asphericity coefficients of all structures relevant for human eye modeling. The pupil has been designed with a 4 mm diameter to simulate a non-mydriatic acquisition with no visible light and is coincident with the lens anterior surface. The chromatic aberrations from the eye were neglected as the change in diopters at different wavelengths were not considered significant in the scope of this work [1].

The refractive indexes for each medium are:

- Cornea: 1.376
- Aqueous Humour: 1.366
- Lens: 1.406
- Vitreous Humour: 1.336

The defined refractive surfaces of the eye, as represented in Fig. 4, are:

- Corneal Anterior surface: Diameter = 11.50 mm
  Radius of Curvature = 7.75 mm
  Asphericity coefficient = −0.2
- Corneal Posterior surface:
  Diameter = 11.50 mm
  Radius of Curvature = 6.8 mm
  Asphericity coefficient = 0
- Pupil/Lens Anterior surface:
  Diameter = 4 mm
  Radius of Curvature = 10 mm
  Asphericity coefficient = −0.94
- Lens Posterior Surface:
  Diameter = 9 mm
  Radius of Curvature = −6 mm
  Asphericity coefficient = 0.96

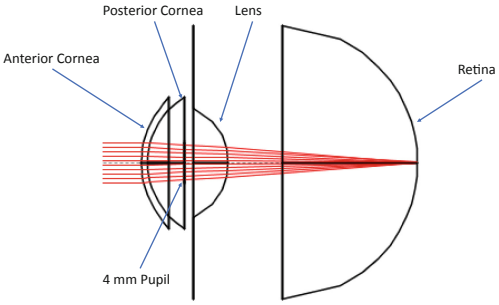

Fig. 4. BEAM IV simulation of the eye model used with collimated rays being focused on the retina [17].

– Retina:
  Diameter = 24 mm
  Radius of Curvature = 12 mm
  Asphericity coefficient = 0

2.2 Illumination Path

For the illumination path the main goal is a 40° field-of-view with a uniform illumination of the retina. The diagram of the illumination path is represented in Fig. 5. The image is obtained using a White LED but, to allow a non-mydriatic acquisition, a Near Infrared (NIR) LED is used, helping the examiner to perform alignment of the device with the eye and to find the area of the retina to be imaged. As in most fundus cameras, there is a lens above the light source to collimate the rays and another lens to focus the rays [30].

To obtain a field-of-view of 40° there is a constraint that the relationship $\frac{WD}{2f}$ should be equal to or larger than sin(20), where WD stands for Working Diameter and f means the effective focal length of the lens. This condition, coupled with the demand of minimization of spherical aberrations makes Aspheric lenses the only suitable option for the focusing of the rays when reaching the retina.

The lenses for the illumination path of the optical system described in this paper were the ones used in Melo et al. [17], a Thorlabs aspheric lens with 50.00 mm diameter, 40.00 mm focal length and SLAH-64 glass type as an objective and for collimation of the light rays an Edmund Optics Plano-Convex Lens with 25.4 mm diameter, 38.1 mm focal length and N-BK7 glass type. Even though the lenses are the same when compared with the optical system, the usage of the polarizer lead to a different placement of both lenses. The condenser lens was brought down so the polarizers could fit the system while the objective lens was placed to the right of its initial position. So, despite using the same set of lenses the optical system shown in Fig. 5, has several different features.

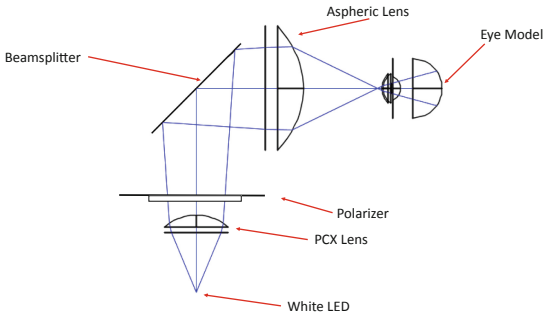

Fig. 5. Visible Light illumination path and components used. (Color figure online)

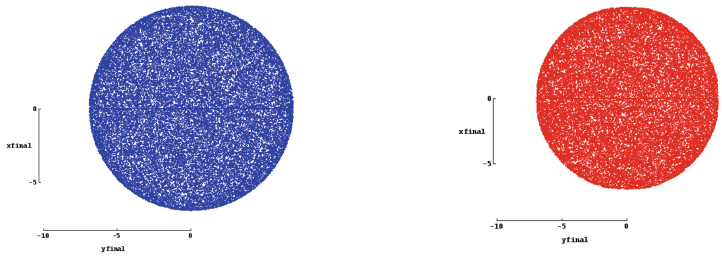

(a) Blue light **(b)** Red light

Fig. 6. The retinal area illuminated, also called retinal illumination profile, is described, for the configuration represented in Fig. 5 at both ends of the visible electromagnetic spectrum. (Color figure online)

As the white light emitted by the LED has a continuous emission spectrum, measurements at both ends of the visible spectrum are needed. The mean percentage of rays for both wavelengths (blue - 486.13 nm, red - 656.27) reaching the retina for the white visible LED, is about 90% of the ones emitted. The illumination profile is uniform, as can be observed in Fig. 6 for blue and red light. The mean value was also calculated between the illumination half-angle of both wavelengths and was 20.58° leading to a total field-of-view of 41.16°.

2.3 Imaging Path

For the imaging path the key features desired are the almost complete fulfillment of the Smartphone Camera sensor angle-of-view, the minimization of aberrations and an accurate focusing of the rays in the retina. In order to perform ray tracing analysis of the imaging path, two pairs of parallel rays going from the smartphone camera to the back of the eye were considered, one pair parallel with the optical axis and the other with an angle close to the value of the vertical angle of view of the smartphone.

The system was optimized for a LG Nexus 5X camera whose relevant specifications are:

- Horizontal Angle of View: 68.2°
- Vertical Angle of View: 53.1°
- Sensor Size: 1/2.3″ (6.17 × 4.55 mm)
- Resolution: 12 Megapixels

The final optical system must guarantee that the Vertical Angle of View is mostly filled with the retinal image, in order to allow the highest possible retinal resolution, essential for the clinical analysis of fine features. The objective lens had already been defined by the simulations of the illumination path so it was necessary to test which lens could best fulfill our needs as an ocular. The solution that we came up was with a Best-Form lens. These lenses are manufactured with a conjunction of curvatures in both surfaces that minimizes monochromatic aberrations. They were proven to operate better in this type of applications than regular Plano-Convex Lenses [17]. So a Best-Form Lens with 40.0 mm focal length, 25.0 Diopters and 25.4 diameter was tested, leading to the imaging path presented in Fig. 7. As for the illumination path, even though the lenses are the same, changes in the relative distance between components were required so the system could physically accommodate polarizers. The use of polarizers will be justified in the Subsect. 2.4. The imaging path is presented in Fig. 7.

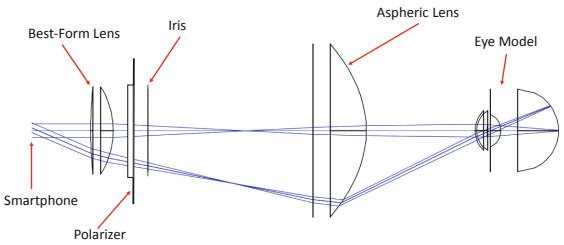

Fig. 7. Parallel rays model. In this model the progression of two pairs of parallel rays is studied, one parallel with the optical axis and the other with an angle of 22°. The goal is to ensure that both pairs have their focal point as close to the retina as possible. In this configuration 83% of the smartphone vertical angle of view is approximately used.

Only 83% of the smartphone vertical angle of view is used because the Best-Form Lenses required for the reduction of spherical aberrations are only available with relatively small diameters, making it difficult to use much wider angles. Besides that 83% of the smartphone camera 12 Megapixels resolution can be considered sufficient for fundus imaging. The iris (or aperture stop) in Fig. 7 has 25 mm of inner diameter and a thickness of 1 mm. Its purpose is to stop the rays at a wider angle than the necessary for a field-of-view of 40°, preventing reflections and the imaging of not illuminated areas of the retina.

2.4 Polarizers

Polarizers are, by definition, optical filters where the transmission of light is dependent on its polarization. Being really helpful to block light with a specific polarization having many application in fields like microscopy and photography. Light reflected from dielectric surfaces, like water, glass or the human cornea has its electrical vector parallel with that surface so get linearly polarized [7].

Polarizers are usually named after the polarization of light transmitted by it. The two most applied types of polarizers are linear and circular. Circular polarizers are composed of one linear polarizer followed by a retarder (or quarter wave-plate). When the angle between the axis of the retarder and the axis of the linear polarizer is 90°, the light becomes circularly polarized being right-handed or left-handed polarized, depending on the relative orientation between components [20].

Taking advantage of the polarization state changes light suffers along the optical path, polarizers can be a great tool in the prevention of undesired reflections from reducing the quality of the final image obtained, ensuring that only light coming from the fundus reach the Smartphone CMOS. Linearly polarized light when reflected from a dielectric surface keeps its polarization state. This property can be explored using one polarizer right above the condenser lens to make light linearly polarized and the other on the imaging path right before the ocular lens. According to several papers light reaching the fundus is scattered on the retina and by other the human eye structures, thus becoming depolarized [4,31]. So polarizers must be perpendicularly oriented so light coming from the illumination path polarizer without any depolarization is blocked. This way, light that is reflected from the cornea and the back of the objective lens, is blocked by the polarizer. Using polarizers this way is often named crossed polarizers technique [30].

2.5 Imaging Path for Eyes with Refractive Errors

Eyes with refractive errors present different optical characteristics and so the distance between lenses in the optical system must be adjustable to compensate this.

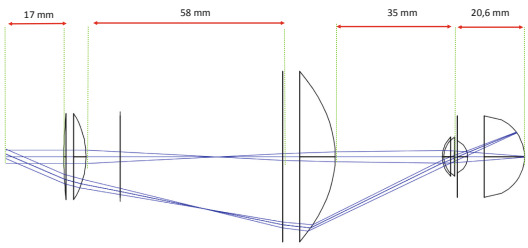

Fig. 8. The distances between each components to image an eye without refractive errors.

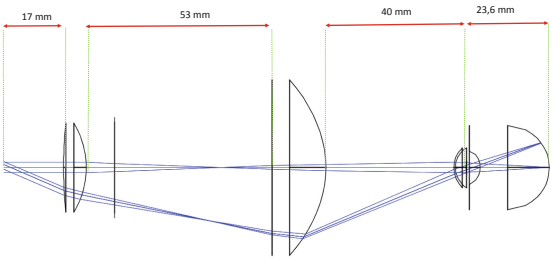

Fig. 9. The distances between each components to image an eye with refractive errors (Myopia).

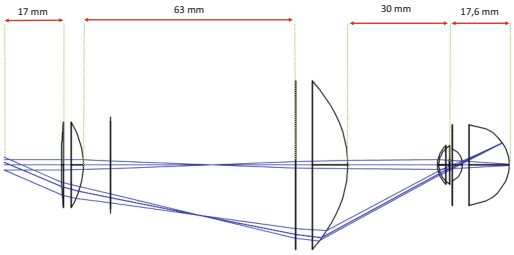

Fig. 10. The distances between each components to image an eye with refractive errors (Hyperopia).

As the smartphone camera is able to change its focus target distance, the refractive errors were only simulated in the range −5D to +5D. Since one of the possible cause of refractive errors is the size of the eyeball, for the simulation of Myopia the retina was moved 3 mm away from the refractive center of the eye. Concerning the simulation of Hyperopia the eyeball was shortened 3 mm.

In Fig. 8, the system configuration for an eye without any refractive error is shown. In Figs. 9 and 10, diagrams showing the adjustments done to compensate these refractive errors are shown.

For the Myopic eye the error is corrected by moving the Objective Lens 5 mm away from the eye.

Concerning the Hyperopic eye, the Objective lens is approximated 5 mm to the eye.

2.6 Mechanical Prototyping

The optical system previously described was implemented in a 3D printed prototype (Figs. 11 and 12). The design of the mechanical prototype was developed using Solid Works. The important goals for this prototype are to allow the arrangement of the desired lens, a support for the smartphone that ensures that the camera is centered with the optical path, and the adjustment of the objective lens. Due to the need of physical space for the placement of polarizers

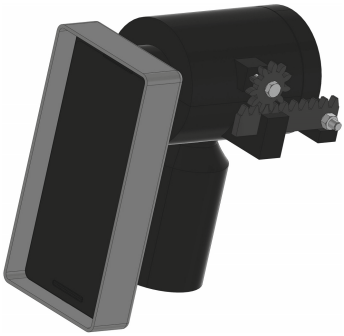

Fig. 11. Mechanical prototype showing both the smartphone support and the rack and pinion mate.

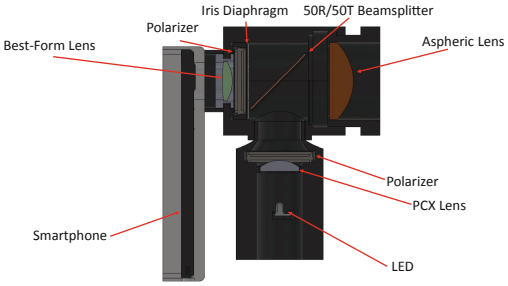

Fig. 12. Section view of the prototype.

and consequent changes on the optical system, when compared with Melo et al. [17] version, several alterations are observable on the 3D printed mechanical prototype. Although some features, like the Rack and Pinion system to allow the examiner to precisely search for the working distance, were preserved.

Other solution to allow the movement of the lens would be by the use of threaded surfaces in both sides, so the rotation of the objective ensures a change in the working distance. This approach was rejected because it is expected the future implementation of a piece leaning against the patient forehead, to guarantee the centering with the Optical Path. The rotation of this piece, in contact with the patient, would not be comfortable or, possibly, safe.

Some other changes were performed in the mechanical prototype design like the implementation of a new case for smartphone support printed in flexible material (FilaFlex) to ensure that smartphone edges weren't damaged. A SolidWorks fastening tool named lip and groove was used in the connection between parts with the goal of preventing external light from entering the mechanical case and create unnatural reflections.

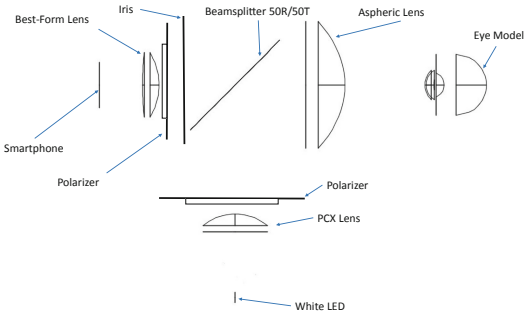

Fig. 13. Complete Optical System.

2.7 Complete System Designed

The Complete System presented in Fig. 13 has the following elements:

- Visible LED - VLHW4100, Ultrabright White LED.
- N-BK7 Plano-Convex Lens, 38.1 mm Focal Length, 25.4 mm ϕ, VIS-NIR Coated.
- S-LAH64 CNC-Polished Aspheric Lens, 40.0 mm Focal Length, 50 mm ϕ.
- Beamsplitter 50R/50T 50 $\times$ 50 mm.
- N-BK7 Best-Form Lens, 40 mm Focal Length, 25.4 mm ϕ.
- Polarizers.

In this setup the distance between the prototype and the human eye is intended to be 31.5 mm.

The main features of the developed system are:

- About 40° field-of-view.
- Non-Mydriatic Acquisition, for a 4 mm pupil size, achievable by using the NIR LED for guidance.
- No significant aberrations (Spherical and Chromatic).
- Uniform Illumination of the Retina.
- Simple and affordable lens system.

3 Handheld Devices Comparison

In this Sect. 3 different handheld devices are compared. To allow an accurate measurement of the Field-of-View, photographs of graph paper are obtained with each of the 3 prototypes. Besides that, images of an eye model (Model Eye Ophthalmoscope Trainer by HEINE) are analyzed and sharpness of the

photographs on specific regions is evaluated. Some post-processing is also applied to the images in order to address the quality of the illumination each prototype supplies. The Optomed Aurora Fundus Camera [18], considered the one with better specifications commercially available wasn't considered in this comparison due to its high cost and low availability.

The three prototypes to be compared are:

- EFS Compact Version;
- EFS Standard Version;
- OICO Fundus Camera.

The prototypes were tested under the same conditions at Fraunhofer Portugal Association facilities in Porto, more specifically in the OpenLab.

3.1 Field-of-View

The Retinal area whose observation is possible is one of the most important features of a Fundus Camera.

The setup for calculation of the FOV comprises a 38.1 mm focal length lens and graph paper. The lens was placed in front of the prototype on the plane where the illumination circle of confusion was minimum and the graph paper was placed in front of the lens at its focal distance (as close to 38.1 mm as possible). The setup for the FOV image acquisition is presented on Fig. 14.

The Total Field of view values obtained for each fundus camera were:

- EFS Compact Version - $45 \times 45°$;
- EFS Standard Version - $45 \times 45°$;
- OICO Fundus Camera - $37 \times 30°$;

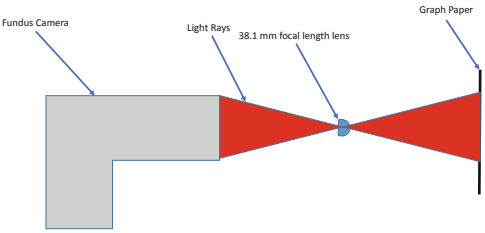

Fig. 14. Diagram of the optical setup for Field of View measurement.

3.2 Eye Model Photos

Images of an eye model were obtained with each one of the 3 different devices. The sharpness of the pictures was qualitatively evaluated and consequently also the suitability of each of the systems for Diabetic Retinopathy Screening. The pictures are shown in Figs. 15 and 16.

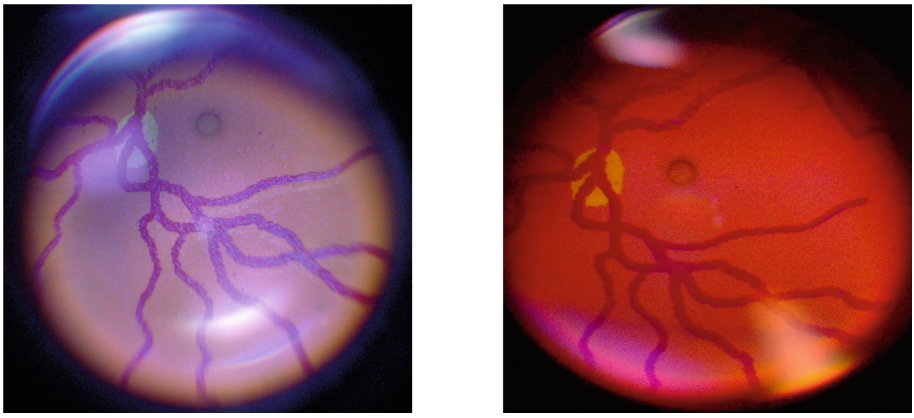

(a) EFS Compact **(b)** EFS Standard

Fig. 15. Model Eye photograph acquired for each EFS prototype.

The differences in the acquirable Field of View as described in the Sect. 3.1 are easily noticeable. The purple spots on the image of the Fig. 15a are caused by back reflections of the objective lens and by reflections from the refractive lens of the eye model, analogous to the cornea in the human eye.

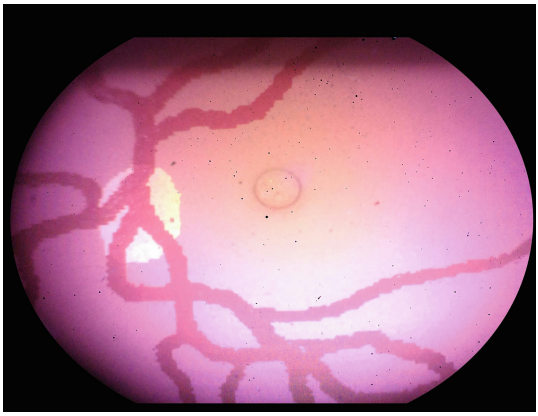

Fig. 16. Model Eye photographs obtained with OICO Fundus Camera.

Even though these reflections can diminish the final quality of the images obtained the sharpness of the image is noticeable when specific regions are zoomed in. Figure 17 allow a comparison between the sharpness of the vessels near the optic disk.

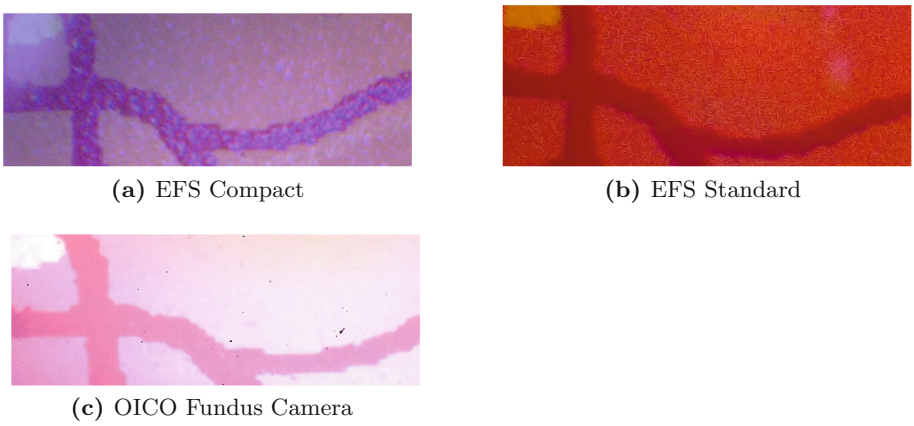

(a) EFS Compact

(b) EFS Standard

(c) OICO Fundus Camera

Fig. 17. Photos acquired with each of the prototypes with zoom in after the acquisition.

The chromatic changes observable on Fig. 17a also show that polarizers are not working properly, as they don't block light coming from the back of the objective lens.

As for the EFS Standard (Fig. 17b), even though, the reflections are not as representative, the illumination intensity seems lower than for the others. Considering the low reflection ratio of the retina, this could be a problem when imaging real human eyes [16].

3.3 Retinal Illumination

To properly illuminate the retina is one of the fundamental challenges when designing a fundus camera, so, a Java open-source software named ImageJ was used to calculate the mean pixel intensity for the images presented in Sect. 3.2. The images were also split in the 3 RGB channels in order to find out any possible saturation and to check the differences between each prototype. As an example, the images obtained for the EFS Standard Eye Model photograph are presented in Fig. 18.

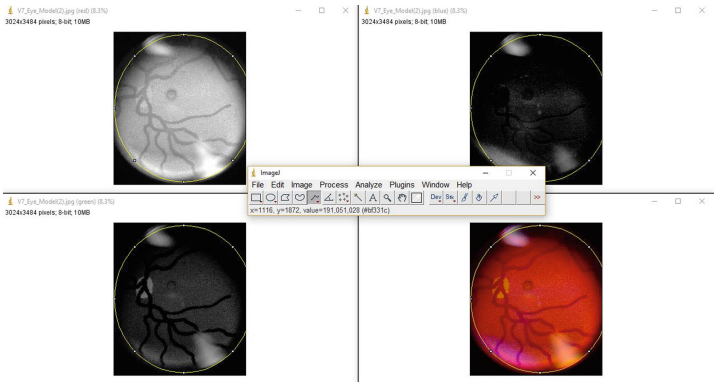

Fig. 18. Eye Model image obtained with the EFS Standard prototype along with its projection on the 3 RGB channels. The yellow line delimits the Region of Interest (ROI) in which the measurement of the pixel intensity were performed. Top Left: Red Channel; Top Right: Blue Channel; Bottom Left: Green; Bottom Right: All channels. (Color figure online)

The red channel of the image obtained with the OICO Fundus Camera presented an artifact at the center of the image, most likely derived from red channel saturation. This problem may be solved by the appliance of a "bluish" White-Balance. White-Balance is a tool normally used to balance the colors, approximating the colors shown in the photographs to the colors of the actual objects. For of Retinal Photography, the normally used White-Balance increases lower wavelengths prevalence over higher wavelengths so, the previously referred red channel saturation effect (Fig. 19) can be minimized [11].

The results obtained for mean pixel intensity on each one of the 3 channels are presented in the following table (Table 1):

Table 1. Comparison on Mean Pixel Intensity for each of the RGB channels using the 3 prototypes.

Prototype	Channel			
	All	Red	Green	Blue
EFS Compact	129	142	100	144
EFS Standard	70	158	30	21
OICO Fundus Camera	180	218	144	177

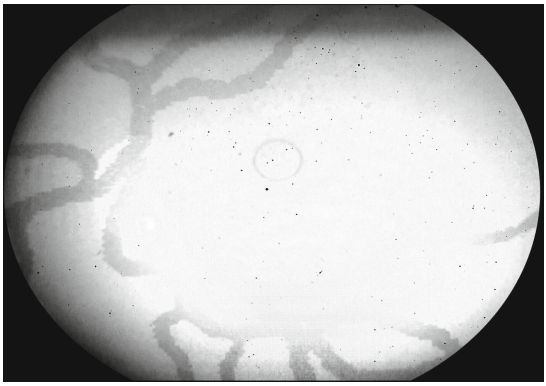

Fig. 19. Red Channel image obtained with the OICO Fundus Camera showing saturation on the middle of photograph.

Besides the calculation of the mean pixel intensity the image was transformed to YUV (in which Y is the variable Luminance, U and V are chromaticity coordinates) so the relative luminance of the 3 images could be directly obtained. As the relative luminance along the object to be imaged (fundus) is not constant (vessels are less bright than retinal epithelium), and the regions of the eye model obtained with each prototype are different, the luminance values presented in Table 2 aren't directly proportional to the illumination intensity. Although, the margin by which they differ, ascertains what was previously predicted on the Sect. 3.2.

Table 2. Comparison on Luminance value for each of the RGB channels using the 3 prototypes.

Prototype	Mean luminance
EFS Compact	0,469
EFS Standard	0,26
OICO Fundus Camera	0,669

The values suggest that OICO Fundus Camera allows an higher illumination intensity than EFS prototypes, and that between EFS prototypes, the EFS Compact has higher illumination intensity than the EFS Compact. The images obtained are presented in Fig. 20.

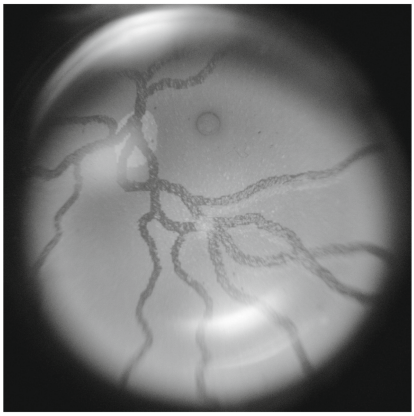

(a) EFS Compact

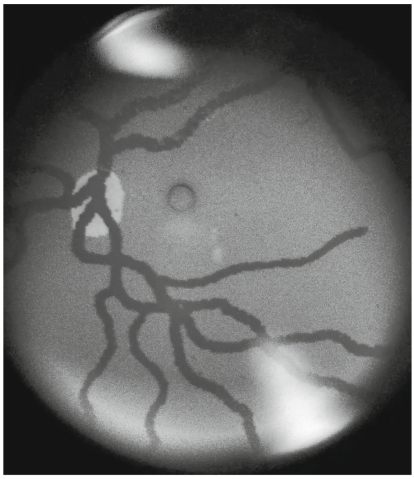

(b) EFS Standard

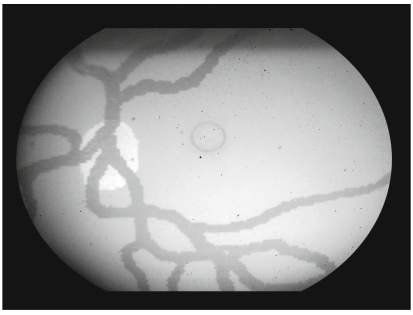

(c) OICO Fundus Camera

Fig. 20. Luminance images for on the photographs of the Fig. 15.

4 Conclusions

Some of the tasks described as future work in Melo et al. [17], were performed and are described in this paper. The Compact prototype has been printed (Fig. 21) and eye model photographs were obtained with the prototype containing the Optical system described in this paper.

The fact that the prototype is 3D-printed (rapid prototyping) supports one of the most important features of the work here presented, the use of the smartphone, for both imaging and processing.

Considering the continuous evolution of smartphone cameras, in the future, this approach may provide a great enhancement on the quality of the images obtained which will, undoubtedly allow an easier detection of fundus structures that regular healthcare personnel, and not only ophthalmologist experts are

Fig. 21. EFS Compact prototype.

aware of. This way, this smartphone-based prototype can become a valuable tool for non-experts.

The fact that the prototype is 3D-printed, besides enforcing rapid prototyping, allows an easier dissemination which could make it a really helpful tool on the prevention of ophthalmic pathologies as: Diabetic Retinopathy (DR), Glaucoma, Age-Related Macular Degeneration, Cardiovascular diseases, Cerebrovascular diseases on medically underserved areas.

It can be concluded that the optical system designed showed satisfactory capabilities in experimental tests, when compared with two other affordable optical systems. The images obtained suggest that the required resolution for the detection of some of the smallest features with interest for Diabetic Retinopathy was achieved.

As future work, to diminish the reflections, an anti-reflective coating should be applied to the lenses, specially on the objective lens, the most likely cause of the purplish blurs on the final image obtained with the Compact Version Fig. 15a. To understand which set of polarizers would help the most on the minimization of back and corneal reflections, an appropriate experimental test set for polarizers comparison should be established and executed. Not only circular, but also linear

polarizers should be tested. The correction of these reflections is considered one major improvement on the reliability of the prototype for real-life use cases.

According to the measurements on Sect. 3.3, and by the observation of Fig. 15b, the illumination light source for the EFS Standard prototype should also be reevaluated so the illumination intensity on the retina can be increased.

Also, features like resolution, illumination uniformity should be addressed with a proper comparison test set in order to acquire measurable information on these handheld systems capabilities for the screening of ophthalmological diseases. Later the results obtained should be compared to the ones regarded for fundus cameras, according to the ISO norm for Fundus Cameras - ISO 10940 [12].

Acknowledgements. We would like to acknowledge the financial support obtained from North Portugal Regional Operational Programme (NORTE 2020), Portugal 2020 and the European Regional Development Fund (ERDF) from European Union through the project Symbiotic technology for societal efficiency gains: Deus ex Machina (DEM), NORTE-01-0145-FEDER-000026.

References

1. Atchison, D., Smith, G.: Optics of the Human Eye, p. 259. Butterworth-Heinemann, Oxford (2000). https://doi.org/10.1016/B978-0-7506-3775-6.50001-8
2. Benbassat, J., Polak, B.C.P., Javitt, J.C.: Objectives of teaching direct ophthalmoscopy to medical students. Acta Ophthalmol. **90**(6), 503–507 (2012). https://doi.org/10.1111/j.1755-3768.2011.02221.x
3. Born, M., Wolf, E.: Principles of Optics, 7th edn. Cambridge University Press, Cambridge (1999)
4. Bueno, J.M.: Depolarization effects in the human eye. Vis. Res. **41**(21), 2687–2696 (2001). https://doi.org/10.1016/S0042-6989(01)00167-5. http://www.sciencedirect.com/science/article/pii/S0042698901001675
5. Bunce, C., Wormald, R.: Leading causes of certification for blindness and partial sight in England & Wales. BMC Public Health **6**, 58 (2006). https://doi.org/10.1186/1471-2458-6-58
6. Cheung, N., Mitchell, P., Wong, T.Y.: Diabetic retinopathy. Lancet **376**(9735), 124–136 (2010). https://doi.org/10.1016/S0140-6736(09)62124-3
7. Cronin, T.W., Shashar, N.: The linearly polarized light field in clear, tropical marine waters: spatial and temporal variation of light intensity, degree of polarization and e-vector angle. J. Exp. Biol. **204**(14), 2461–2467 (2001). http://jeb.biologists.org/content/204/14/2461
8. Cunha-Vaz, J.: Characterization and relevance of different diabetic retinopathy phenotypes. Dev. Ophthalmol. **39**, 13–30 (2007). https://doi.org/10.1159/000098497
9. D-EYE S.r.l.: D-EYE Ophthalmoscope. https://www.d-eyecare.com/#vision
10. Giancardo, L.: Automated fundus images analysis techniques to screen retinal diseases in diabetic patients. Docteur de l ' université Automated Fundus Images Analysis Techniques to Screen Retinal Diseases in Diabetic Patients (2012)
11. Hubbard, L.D., et al.: Brightness, contrast, and color balance of digital versus film retinal images in the age-related eye disease study 2. Invest. Ophthalmol. Vis. Sci. **49**(8), 3269 (2008). https://doi.org/10.1167/iovs.07-1267

12. Ophthalmic instruments - Fundus cameras. Standard, International Organization for Standardization, Geneva, CH (2009)
13. Jenkins, F., White, H.: Fundamentals of Optics. McGraw-Hill, New York (1957). https://books.google.pt/books?id=SAwJAQAAIAAJ
14. Jin, K., Lu, H., Su, Z., Cheng, C., Ye, J., Qian, D.: Telemedicine screening of retinal diseases with a handheld portable non-mydriatic fundus camera. BMC Ophthalmol. **17**(1), 89 (2017). https://doi.org/10.1186/s12886-017-0484-5
15. Kauppi, T.: Eye Fundus Image Analysis for Automatic Detection of Diabetic Retinopathy (2010)
16. van de Kraats, J., Berendschot, T.T., van Norren, D.: The pathways of light measured in fundus reflectometry. Vis. Res. **36**(15), 2229–2247 (1996). https://doi.org/10.1016/0042-6989(96)00001-6
17. Melo, D., Costa, J., Soares, F., Vieira, P.: Optical design of a compact image acquisition device for mobile diabetic retinopathy screening. In: Proceedings of the 11th International Joint Conference on Biomedical Engineering Systems and Technologies, BIODEVICES, vol. 1, pp. 63–70. INSTICC, SciTePress (2018). https://doi.org/10.5220/0006592200630070
18. Optomed Oy Ltd.: Optomed Aurora. https://www.optomed.com/optomedaurora
19. Patton, N., Aslam, T., MacGillivray, T., Pattie, A., Deary, I.J., Dhillon, B.: Retinal vascular image analysis as a potential screening tool for cerebrovascular disease: a rationale based on homology between cerebral and retinal microvasculatures. J. Anat. **206**(4), 319–348 (2005). https://doi.org/10.1111/j.1469-7580.2005.00395.x. http://www.ncbi.nlm.nih.gov/pmc/articles/PMC1571489/, 15817102[pmid]
20. Peli, E.: Ophthalmic applications of circular polarizers. J. Am. Optom. Assoc. **57**, 298–302 (1986)
21. Pérez, M.A., Bruce, B.B., Newman, N.J., Biousse, V.: The use of retinal photography in non-ophthalmic settings and its potential for neurology. Neurologist **18**(6), 350–355 (2012). https://doi.org/10.1097/NRL.0b013e318272f7d7. http://www.ncbi.nlm.nih.gov/pmc/articles/PMC3521530/, 23114666[pmid]
22. Phillips, C.I.: Dilate the pupil and see the fundus. Br. Med. J. (Clin. Res. Ed.) **288**(6433), 1779–1780 (1984). http://www.ncbi.nlm.nih.gov/pmc/articles/PMC1441835/, 6428541[pmid]
23. do Prado, R.S., Figueiredo, E.L., Magalhaes, T.V.B.: Retinal detachment in preeclampsia. Arquivos brasileiros de cardiologia **79**(2), 183–186 (2002). https://doi.org/10.1590/S0066-782X2002001100011. http://ovidsp.ovid.com/ovidweb.cgi?T=JS&PAGE=reference&D=med4&NEWS=N&AN=12219193
24. Quellec, G., Bazin, L., Cazuguel, G., Delafoy, I., Cochener, B., Lamard, M.: Suitability of a low-cost, handheld, nonmydriatic retinograph for diabetic retinopathy diagnosis. Transl. Vis. Sci. Technol. **5**(2), 16 (2016). https://doi.org/10.1167/tvst.5.2.16
25. Salz, D.A., Witkin, A.J.: Imaging in diabetic retinopathy. Middle East Afr. J. Ophthalmol. **22**(2), 145 (2015)
26. Shen, B.Y., Mukai, S.: A portable, inexpensive, nonmydriatic fundus camera based on the raspberry pi® computer. J. Ophthalmol. **2017**(3), 5 (2017). https://doi.org/10.1155/2017/4526243. http://www.sciencedirect.com/science/article/pii/S0022231399005992
27. Swedish, T., Roesch, K., Lee, I., Rastogi, K., Bernstein, S., Raskar, R.: EyeSelfie: self directed eye alignment using reciprocal eye box imaging. ACM Trans. Graph. **34**(4), 58 (2015)

28. Tarr, J.M., Kaul, K., Chopra, M., Kohner, E.M., Chibber, R.: Pathophysiology of diabetic retinopathy. ISRN Ophthalmol. **2013**, 1–13 (2013). https://doi.org/10.1155/2013/343560
29. Tocci, M.: How to model the human eye in zemax (2007). http://www.zemax.com/kb/articles/186/1/How-to-Model-the-Human-Eye-in-ZEMAX/Page1.html
30. Tran, K., Mendel, T.A., Holbrook, K.L., Yates, P.A.: Construction of an inexpensive, hand-held fundus camera through modification of a consumer "point-and-shoot" camera. Invest. Ophthalmol. Vis. Sci. **53**(12), 7600–7607 (2012)
31. Tuchin, V.V.: Polarized light interaction with tissues. J. Biomed. Opt. **21**, 1–37 (2016). https://doi.org/10.1117/1.JBO.21.7.071114
32. Volk Optical Inc.: Volk InView. https://volk.com/index.php/volk-products/ophthalmic-cameras/volk-inview.html
33. Volk Optical Inc.: Volk Pictor Plus. https://volk.com/index.php/volk-products/ophthalmic-cameras/volk-pictor-plus-digital-ophthalmic-imager.html